



Power Electronic Systems
Laboratory

© 2017 IEEE

IEEE Transactions on Industry Applications, Vol. 53, No. 3, pp. 2077-750-2087, May/June 2017

Advanced Cooling Methods for High-Speed Electrical Machines

A. Tüysüz,
F. Meyer,
M. Steichen,
C. Zwyssig,
J. W. Kolar

This material is published in order to provide access to research results of the Power Electronic Systems Laboratory / D-ITET / ETH Zurich. Internal or personal use of this material is permitted. However, permission to reprint/republish this material for advertising or promotional purposes or for creating new collective works for resale or redistribution must be obtained from the copyright holder. By choosing to view this document, you agree to all provisions of the copyright laws protecting it.



Eidgenössische Technische Hochschule Zürich
Swiss Federal Institute of Technology Zurich

Advanced Cooling Methods for High-Speed Electrical Machines

Arda Tüysüz, *Member, IEEE*, Francesca Meyer, Mathis Steichen, Christof Zwyssig, *Member, IEEE*, and Johann W. Kolar, *Fellow, IEEE*

Abstract—High-speed electrical machines are gaining increasing attention, as they enable higher power densities in several applications such as micromachining spindles and turbo compressors. This brings along an important challenge in thermal management due to the higher loss densities in the machine. Therefore, a careful thermal analysis is required along with the electromagnetic and mechanical considerations during the design phase of the machines. In this paper, different forced cooling options are compared for a slotless-type high-speed permanent-magnet machine. Fast, yet sufficiently accurate thermal models are derived for analyzing these cooling concepts. This enables their coupling with electromagnetic models and incorporation into the machine optimization procedure, which would not be feasible when using computationally very intensive methods such as three-dimensional finite element method or computational fluid dynamics. The developed thermal models are first verified on mechanically simplified stator designs (in which no rotor coupling is possible), and later on fully functional high-speed electrical machine prototypes. Using an integrated cooling method instead of a standard cooling jacket, the power density can be nearly doubled while keeping the maximum winding temperature below 80 °C, without altering the rotor or the stator core geometries.

Index Terms—Cooling, high-power-density drives, high-speed drives, modeling, slotless machine.

I. INTRODUCTION

DEE TO the higher power density that they offer, high-speed drives have been a very popular research topic lately, both in academia and industry. Furthermore, a major part of the

Manuscript received August 11, 2016; revised December 23, 2016; accepted February 12, 2017. Date of publication February 22, 2017; date of current version May 18, 2017. Paper 2016-EMC-0530.R1, presented at the 2015 9th International Conference on Power Electronics and Energy Conversion Congress and Exposition (ECCE) Asia, Seoul, South Korea, Jun. 1–5, and approved for publication in the IEEE TRANSACTIONS ON INDUSTRY APPLICATIONS by the Electric Machines Committee of the IEEE Industry Applications Society.

A. Tüysüz and J. W. Kolar are with the Power Electronic Systems Laboratory, Swiss Federal Institute of Technology (ETH) Zurich, Zurich 8092, Switzerland (e-mail: tuysuz@lem.ee.ethz.ch; kolar@lem.ee.ethz.ch).

F. Meyer was with the Power Electronic Systems Laboratory, Swiss Federal Institute of Technology (ETH) Zurich, Zurich 8092, Switzerland. She is now with ABB Switzerland, Baden 5400, Switzerland (e-mail: francesca.meyer@ch.abb.com).

M. Steichen was with the Power Electronic Systems Laboratory, Swiss Federal Institute of Technology (ETH) Zurich, Zurich 8092, Switzerland. He is now with the Interdisciplinary Centre for Security, Reliability, and Trust, University of Luxembourg, Luxembourg 2721, Luxembourg (e-mail: mathis.steichen@uni.lu).

C. Zwyssig is with Celeroton Ltd., Zurich 8092, Switzerland (e-mail: christof.zwyssig@celeroton.com).

Color versions of one or more of the figures in this paper are available online at <http://ieeexplore.ieee.org>.

Digital Object Identifier 10.1109/TIA.2017.2672921

research about electrical machinery is expected to be about high-speed drives in the near future [1], due to both the advancements in enabling technologies (e.g., magnetic [2] and gas bearings [3], higher quality core materials [4], self-sensing techniques for low-salinity machines [5]) and the advantages that high-speed drives bring in several emerging applications such as portable power generators, turbo compressors, and spindles [6], [7].

The miniaturization enabled by high rotational speeds is especially beneficial in heating, ventilation, and air conditioning in mobile applications, as well as turbocharging of higher efficiency, more-electric drivetrains of automobiles [1]. For instance, a 500 000 r/min, 150 W electrically driven turbo compressor is proposed in [8] for the cabin pressurization of a solar-powered airplane. Similarly, higher rotational speeds are shown to enable significant weight reduction in reaction wheels used for attitude control of small satellites in [9].

In high-speed drives, besides increased mechanical stresses in the rotor and rotor dynamics constraints, thermal considerations become more important due to the higher loss densities resulting from a smaller volume and surface area. In order to design a reliable and optimum machine, the traditional way of optimization considering only electromagnetic and mechanical aspects for a given specific electric loading cannot be taken anymore, and the thermal design needs to be part of the machine design procedure [10]. Different examples of combined thermal and electromagnetic analyses of electric machines are discussed in [11]–[13]. A comprehensive review of modern cooling systems applied to electrical machines is given in [14].

The slotless permanent-magnet (PM) machine topology (see Fig. 1) is usually preferred for high-speed drives (above 200 000 r/min), due to its weak armature field caused by the large magnetic air gap, which in turn leads to lower rotor losses. Furthermore, the slotless configuration means that stator core saturation or demagnetization of the PM rotor is possible only by having unpractically high current densities in the windings. Therefore, temperature rise is the main factor that limits the rated power of a given slotless high-speed machine, whose maximum safe operating speed is set by rotor dynamics and mechanical stresses in the rotor. Consequently, the torque density and hence the power density of the machine can be increased by using a higher performance cooling system.

If the only load-dependent loss component of an electrical machine is assumed to be Joule losses in the windings, and other loss components such as core, windage, and bearing losses are assumed to be only a function of the rotor speed, it becomes

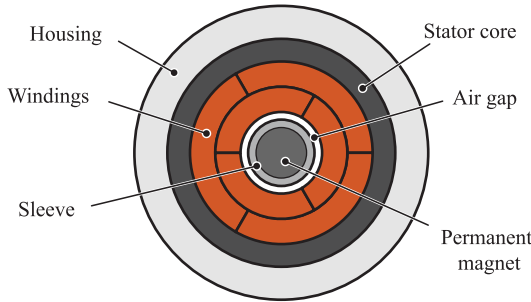


Fig. 1. Conceptual representation of the cross-sectional area of a slotless PM machine with skewed-type air gap windings. The windings are depicted symmetrically (one inner and one outer layer coil side per phase); however, in practice it may look differently depending on the axial location of the cross-sectional view.

clear that increasing the power output of a machine by providing a higher cooling performance results in a reduction of efficiency. However, in certain applications, such as machining spindles, where the size of the tool head limits the shape of possible work pieces, a lower efficiency may be accepted in order to increase the power density further. Moreover, in mobile applications such as turbo compressors in aircraft or road vehicles, an electrical machine with higher power density, albeit itself having a relatively low efficiency, may be desirable due to the weight reduction it enables. Therefore, this work is focused on the power density improvement of high-speed, slotless, PM electrical machines using different forced cooling methods.

Initial considerations on the cooling of high-speed electrical machines have been discussed in [15], where several different forced cooling concepts for a slotless-type high-speed PM machine are described, considering both air and water as coolants. Fast, yet sufficiently accurate thermal models have been derived for describing these forced cooling methods such that the cooling system analysis could be made part of the machine optimization procedure, which is not always feasible with the computationally very intensive methods such as three-dimensional (3-D) finite-element method (FEM) or computational fluid dynamics (CFD). Moreover, the validity of the thermal models has been shown in [15], by measurements taken on different stators that are manufactured by integrating the analyzed forced cooling methods into an off-the-shelf 280 000 r/min, 1 kW electric machine by keeping the original magnetic design. However, since they were manufactured solely for the verification of the thermal models, the mechanical design of these stators did not permit a rotor to be employed.

This paper recaps the main aspects of [15], which provides the basis for a subsequent analysis of the power density increase of an actual electrical machine enabled by integrated forced cooling. Different forced cooling methods are briefly introduced, and they are compared both using models and measurements. Then, an integrated design work flow is introduced, in which the thermal and electromagnetic models are coupled to each other. Following this modeling approach, two fully functional machine prototypes are constructed, one featuring the state-of-the-art jacket cooling and the other with an integrated annular gap cooling. The maximum achievable power densities of both

TABLE I
KEY PARAMETERS OF THE CONSIDERED MACHINE

Rated speed	280 000 r/min
Rated power	1 kW
Pole pair number	1
Rated efficiency	0.94
PM flux linkage	1.75 mVs
Phase resistance	0.14 Ω
Phase inductance	10 μH
Rotor diameter	11 mm
Stator diameter	27.5 mm
Winding bore diameter	12.5 mm
Axial length	33 mm

machines are compared. Only water is considered as coolant in this work due to its better cooling capability compared to air, its easy handling and its wide availability. Measurements taken with these prototypes verify the improvement of the cooling performance and consequently the feasible increase of power density.

II. THERMAL MODELING OF SLOTLESS PM MACHINES

Methods for thermal analysis of electrical machines can be grouped into lumped-parameter networks, FEM and CFD [16], [17]. The latter two can be used to model complicated geometries and/or various coolant flow conditions. On the other hand, these numerical methods are computationally very intensive; hence, it is impractical to integrate them into the initial machine optimization phase, where a large amount of design points need to be evaluated. Lumped-parameter approaches, on the other hand, offer a computationally efficient thermal analysis method, in which the electrical machine geometry can be discretized in cuboidal [18] or arc-segment-shaped [19] elements, and the thermal behavior can be analyzed by solving a thermal equivalent network. For that reason, in this work, a lumped-parameter-based method is adopted for thermal analysis, with the goal of developing a computationally inexpensive thermal model that can be integrated in the machine optimization procedure, while still yielding reasonably accurate results.

A conceptual representation of the slotless PM machine topology is shown in Fig. 1. The stator core is made of a hollow-cylinder-shaped stack of laminated amorphous iron (sheet thickness $\approx 20 \mu\text{m}$). Skewed-type air gap windings [20] made of litz wire are used in order to limit the axial space required for the end windings. Windings and the stator core are bound using epoxy casting. The rotor consists of a diametrically magnetized cylindrical PM, and a retaining sleeve made of titanium. The sleeve ensures mechanical stability and also transfers the torque to the load of the machine by forming a shaft at the axial ends of the rotor. Table I summarizes key design parameters of the machine considered in this work [21].

For modeling the thermal behavior of the machine, its geometry is discretized in all three dimensions¹ using cylindrical

¹For modeling the machines with a cooling setup that is symmetric around the azimuthal axis, an axisymmetric 2-D model can be used instead of a 3-D model. However, the model is developed in 3-D here for generality. Only one element can be used in the azimuthal direction in case of axisymmetric setups for further decreasing the computational effort.

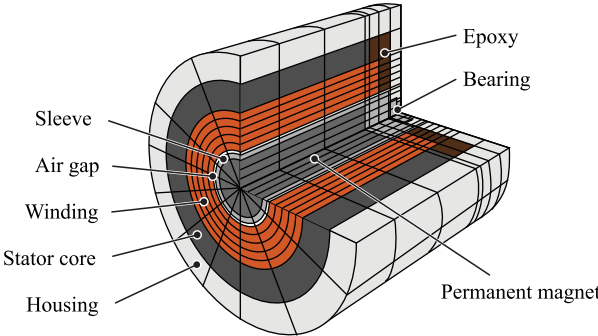


Fig. 2. Discretization of the machine geometry for thermal analysis. Only three quarters of the axial half of the complete machine geometry is illustrated.

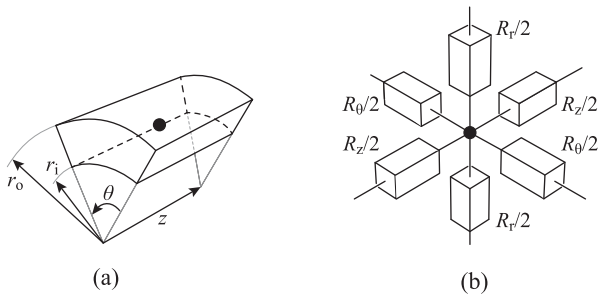


Fig. 3. (a) Basic arc-shaped thermal element that is used to discretize the machine geometry. (b) Representation of the arc-shaped thermal element with respect to its center node and six thermal resistances in radial (r), axial (z), and azimuthal (θ) directions.

coordinates as shown in Fig. 2. This results in the representation of the machine geometry by a set of small arc-shaped elements as shown in Fig. 3(a). For solid domains, where heat is transferred by conduction, each arc-shaped element is further divided into two halves in all three axes as shown in Fig. 3(b), and (1)–(3) are used to calculate the values of the thermal resistances in radial ($R_{\text{th},r}$), axial ($R_{\text{th},z}$), and azimuthal² ($R_{\text{th},\theta}$) directions

$$R_r = \frac{\ln(r_o/r_i)}{\lambda_r \theta z} \quad (1)$$

$$R_z = \frac{2z}{\lambda_z \theta (r_o^2 - r_i^2)} \quad (2)$$

$$R_\theta = \frac{\theta (r_o^2 - r_i^2)}{2\lambda_\theta z (r_o - r_i)^2} \quad (3)$$

where r_o , r_i , z , and θ define the arc shape [cf. Fig. 3(a)]. λ_r , λ_z , and λ_θ are the specific thermal conductivities of the material in the radial, axial, and azimuthal directions, respectively.

In this representation, the center node coincides with the geometric center of the arc-shaped element. The losses associated with that element (e.g., copper losses, if the element is representing a part of the windings) are introduced at the center node, considering the loss density in the machine and the volume of that specific element. Anisotropic thermal conductivities of the laminated stator core or the winding pack can easily be

²The azimuthal thermal resistance depends on the radius where it is evaluated. Here, the mean radius is used.

TABLE II
SPECIFIC THERMAL CONDUCTIVITIES (W/mK)

	$\lambda_{r,w}$	2.1
Winding pack ⁱ	$\lambda_{z,w}$	60
	$\lambda_{\theta,w}$	2.1
	$\lambda_{r,c}$	9
Stator core [22]	$\lambda_{z,c}$	5
	$\lambda_{\theta,c}$	9
Housing [23]	λ_h	235
Epoxy [24]	λ_e	0.85
Sleeve [25]	λ_s	22
Permanent magnet [26]	λ_m	10

ⁱMeasured on an epoxy-cast skewed-type air gap winding.

accounted for by applying different specific thermal conductivity values in different axes. Table II summarizes the specific thermal conductivities of different parts of the machine.

The thermal interfaces between different machine domains are considered based on the nominal manufacturing tolerances of the machine assembly. An epoxy layer of 0.3 mm with a thermal conductivity of 0.85 W/mK between the core and housing represents the small volume at the clearance between those two domains that will be filled up by epoxy during casting. Similarly, the clearance between the winding and the core is assumed to be filled with a 0.1 mm epoxy layer. Additionally, a 0.06 mm of polyimide tape with a thermal conductivity of 0.026 W/mK is present between the winding and the core, which is also included in the thermal model.

Following the treatment of the conductive heat transfer and the heat sources, the convective heat transfer that takes place in the air gap and in the forced cooling channels needs to be treated for finalizing the thermal model. The rate of heat transfer to the coolant flow can be calculated by CFD and modeled as a thermal resistance element within the thermal network described above [27]. However, this would increase the computational effort and go against the goal of having a fast model. Therefore, an alternative method is adopted in this work, where the empirical heat transfer correlations presented in the literature are used with the help of dimensionless numbers that enable their application to the machine geometry and coolant flow conditions at hand. The Nusselt number Nu can be obtained from [28] for cooling channels having the form of either round-shaped ducts or annular gaps, based on whether the coolant flow is laminar, mixed, or turbulent. The equivalent thermal resistance R_{fl} to the coolant is then calculated based on the heat transfer coefficient h as

$$h = \frac{Nu \lambda_{\text{fl}}}{d_{\text{h}}} \quad (4)$$

$$R_{\text{fl}} = \frac{1}{h A_{\text{we}}} \quad (5)$$

where d_{h} is the hydraulic diameter of the channel, A_{we} is the wetted surface, and λ_{fl} is the thermal conductivity of the coolant [28]. The thermal conductivity of the air gap is calculated according to [29], taking the rotational speed of the rotor into account.

Convective heat transfer is more complicated to analyze compared to its conductive counterpart, due to the need of iterative

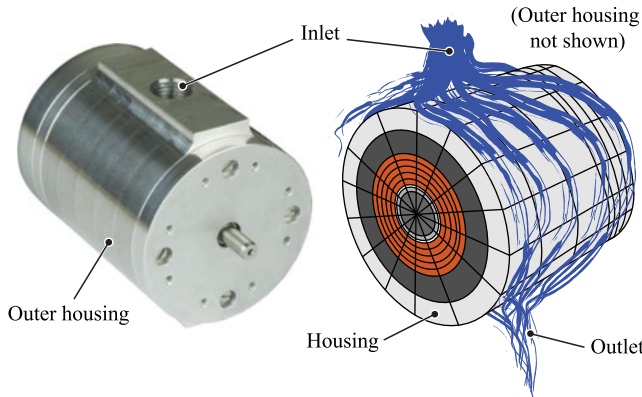


Fig. 4. Jacket cooling method, which is the state-of-the-art cooling method employed in the off-the-shelf electrical machine that is used in this work [21]. Even though it simplifies the design by decoupling the thermal and electromagnetic design, this type of cooling results in a suboptimal cooling performance.

computation (cf. Fig. 13). The analysis starts with the initialization of the fluid temperature in the cooling channel. The thermal resistance to the coolant is calculated based on the wall surface and the fluid temperatures as well as the fluids physical properties. With this, the heat transfer to/from the fluid is calculated, resulting in a change in the fluid temperature. This is repeated with the updated fluid temperature until the results converge.

Once the geometric discretization is carried out and the thermal resistance network is set up, the next step is the addition of the heat sources. As will be revisited in Section IV, the loss components considered in this work are the stator core losses, copper losses (including skin and proximity effects), and windage losses, which are assigned in the nodes belonging to the stator core, winding, and air gap regions, respectively. Finally, the steady-state temperature of each element is found by solving the system as described in detail in [30].

III. FORCED COOLING METHODS

A. Jacket Cooling

Jacket cooling is a widely used cooling method, which is also employed in the off-the-shelf electrical machine that is used in this work as a case study. In this method, the coolant flows outside the machine housing as shown in Fig. 4. The electromagnetic design of the machine is decoupled from the cooling system design, i.e., a cooling jacket can be built around any machine that has been optimized considering only electromagnetic and mechanical aspects. However, this results in a suboptimal cooling performance, as the thermal interface between the coolant and the critical parts of the machine (windings and PM) has a relatively high thermal resistance. The collection of empirical formulas describing the convective heat transfer into coolants flowing in widely used channel shapes (as summarized in [28]) cannot be applied to the jacket cooling method considered in this work due to the significantly different channel geometry. However, as a result of the large cooling contact surface with the coolant, and also assuming the coolant flow rate and the machine efficiency are sufficiently high, jacket cooling

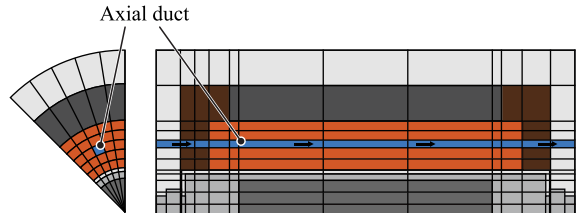


Fig. 5. Representation of the machine geometry for the thermal analysis of the machine with axial ducts.

can be modeled in the first step as a fixed temperature (temperature of the coolant) on the outermost boundary of the housing (i.e., by imposing a fixed voltage on the nodes representing this boundary in the thermal equivalent network). The discretization of the geometry is carried out considering the tradeoff between the computational effort and an adequate representation of the machine's thermal behavior; the geometry is discretized using 13 radial and 11 axial elements.

B. Axial Ducts

In a slotless high-speed electrical machine, copper losses are the loss component that has the strongest dependency on the torque of the machine (for instance, doubling the torque of the machine nearly quadruples the copper losses). Therefore, the thermal connection between the winding region and the coolant needs to be improved for increasing the torque, and hence the power output of the machine. An approach to cool the winding region is to bring the coolant flow closer to the windings. One way of doing this is by introducing axial ducts in the winding region [31]. This clearly decreases the overall thermal resistance toward the coolant and hence decreases the temperature of the hotspots. On the other hand, it increases the copper losses, as the total winding cross-sectional area is reduced for the same stator diameter. Therefore, the number and size of the axial ducts need to be optimized considering the tradeoff between the heat transfer rate and copper losses. In this work, 12 axial ducts are considered, each with a 1 mm^2 cross-sectional area.

Fig. 5 shows the model used to study the thermal behavior of the machine with axial ducts. In the azimuthal direction, the machine is divided into as many pieces as the number of axial ducts, and the symmetry is utilized. The geometry is discretized into 13 elements in the radial, 12 elements in the axial and 5 elements in the azimuthal direction. The axial ducts are manufactured by inserting plastic rods with the same cross-sectional area as the ducts into the winding pack during winding, and removing them after epoxy casting.

C. Annular Gap

A further method of bringing the coolant in the active region of the electrical machine is by introducing an annular gap between the winding and the air gap of the machine. Doing so, the coolant is also brought closer to the rotor and therefore the heat is more easily removed from the rotor (via the air gap). The annular gap is separated from the air gap via a thin plastic can such that liquid coolants can be used without wetting the rotor

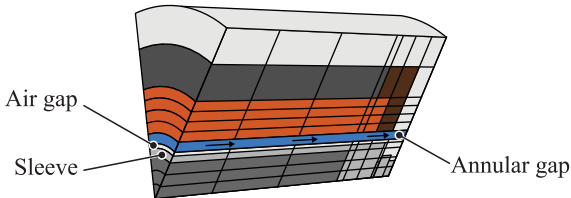


Fig. 6. Representation of the machine geometry for the thermal analysis of the machine with an annular gap.

and/or the bearings; or air can be used without an increase in the windage losses in the air gap.

Keeping the air gap and the stator core geometries constant, the introduction of an annular gap results in a decrease in the winding area. Therefore, similar to the axial ducts, the annular gap has to be dimensioned considering the tradeoff between the thermal performance and the increase in copper losses. The annular gap considered in this work is 0.5 mm thick. Fig. 6 shows the model describing the machine with an annular gap. The geometry is represented by 14 elements in the radial and 12 elements in the axial direction.

D. Further Methods

As described above, bringing the coolant flow into the active region of the electrical machine increases the cooling performance, but decreases the cross-sectional area of the windings for a given inner diameter of the stator core. Alternatively, thermally low-resistive paths (heat pipes) may be provided from the active region of the machine toward the coolant that flows outside the active region. The use of straight, toroidal windings instead of skewed air gap windings and utilizing the high thermal conductivity of the windings in the axial direction has been analyzed in [15]. Even though this arrangement leads to a higher torque-per-ampere ratio due to lack of skew, more than half the total copper length is not used for torque production but contributes to copper losses. As a further alternative, the use of thin (0.1 mm) graphite sheets as heat pipes is discussed in [15]. However, both these methods require a significant modification of the machine manufacturing procedure, and hence are not discussed further.

E. Hardware Design and Comparison of Cooling Concepts

In order to verify the validity of the thermal modeling approach and to compare the integrated cooling methods to the state-of-the-art jacket cooling, three stators are manufactured, each featuring one of these cooling methods. PT-100 temperature sensors are added in the winding as shown in Fig. 7, and hand-held digital multimeters (Fluke 187) are used to measure the temperatures. In order to simplify the manufacturing process, sensors are placed only at the center and one edge in the axial direction. However, the measurements can be repeated by reversed coolant flow direction in order to see the temperatures at coolant inlet and outlet sides of the machine. For the stator employing axial ducts, the azimuthal position is adjusted to measure the hotspot temperatures (e.g., sensor placed in the middle between two axial ducts).

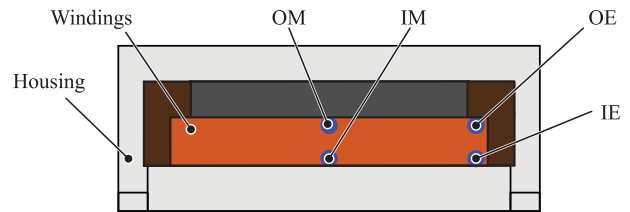


Fig. 7. Placement of the temperature sensors in the winding region for the experimental verification of the thermal models. The rotor and the bearings are not required for the measurements and therefore not considered in the hardware design. The temperature sensors are named according to their location where O, I, E, and M stand for outer, inner, end, and middle, respectively.

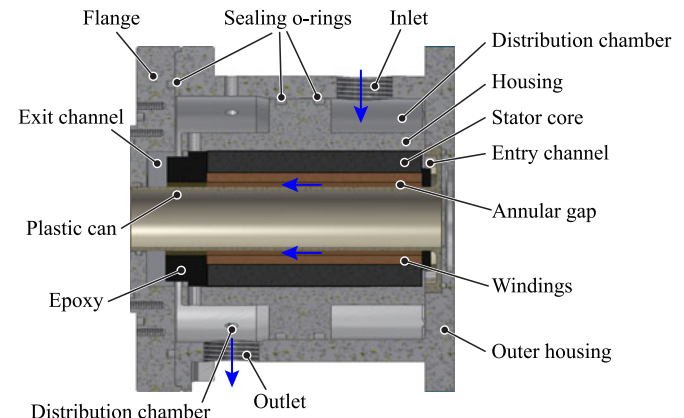


Fig. 8. Construction of the annular gap cooling (not drawn in actual scale or proportions). The coolant is distributed in the tangential direction in a distribution chamber before entering the annular gap through six different channels distributed along the tangential direction (perpendicular to the page plane). The coolant then flows in the annular gap between the winding pack and the 3-D printed plastic can, which separates the annular gap from the air gap. Blue arrows denote the coolant flow path in the cut plane. The thickness of the annular gap is ensured by the positioning of the plastic can in the outer housing and the flange on both axial ends.

As the main goal is the verification of the thermal models and comparison of the cooling methods, the following measurement approach is undertaken. A dc voltage is applied to the windings in order to generate copper losses. The required amount of losses is maintained by adjusting the voltage considering the temperature-dependent electrical resistances of the windings. This removes the uncertainty of the different loss components such as windage losses and allows for a precise verification of the thermal models on the stator side. Rotors are not required for these tests; therefore, the manufactured machine housings do not contain features for accommodating bearings, in order to simplify the production. The stator bore is filled with thermal insulation material in order to maintain an effective adiabatic boundary condition in the experiments.³ Air gap thermal conductivity is set to zero, and only copper losses are considered in the thermal model in order to mimic this measurement condition.

Fig. 8 visualizes how the annular gap cooling is constructed. The coolant inlet and outlet use the same connectors as the

³Repeating those measurements without the thermal insulation material inside the stator bore resulted in similar temperature readings.

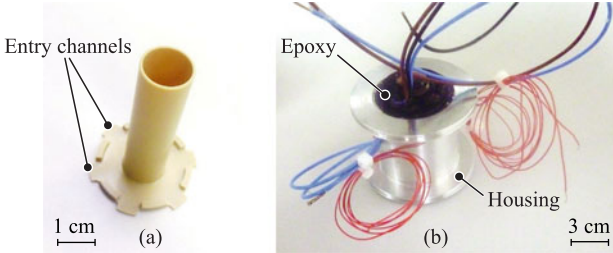


Fig. 9. (a) Plastic can separating the annular gap and the air gap. (b) Photo of the stator with jacket cooling.

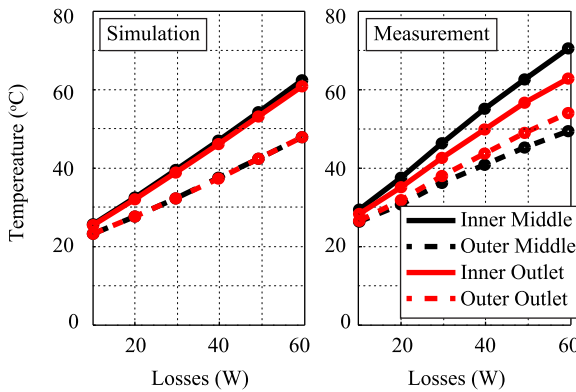


Fig. 10. Simulated and measured winding temperatures for jacket cooling and 1 l/min water flow. Solid lines denote inner and dashed lines denote outer sensors (radial direction). Black denotes the middle and red denotes the outlet side (axial direction). The relative difference of the simulated and measured slopes are 9.2% for the inner middle, 2.2% for the inner outlet, 10.8% for the outer outlet, and 6.8% for the outer middle sensor locations.

jacket cooling for compatibility. The coolant is distributed in the tangential direction in a distribution chamber before entering the annular gap through six different channels distributed along the tangential direction. The coolant then flows in the annular gap between the windings and the 3-D printed plastic can that separates the annular gap from the air gap, which is depicted in Fig. 9 along with the complete stator assembly featuring jacket cooling.

Figs. 10–12 show simulated and measured winding temperatures for jacket cooling, axial duct cooling, and annular gap cooling, respectively. The coolant is 17 °C water with 1 l/min flow rate in all three cases. As predicted by the simulations and verified by measurements, the highest temperature gradient occurs in the radial direction in the case of jacket cooling. A winding hotspot temperature reduction of 40 °C is possible for the same coolant flow rate by incorporating one of the two integrated cooling concepts instead of the standard jacket cooling.

The mismatch between the models and the measurements is attributed to the difference between the actual flow conditions and the geometry of the prototypes and the measurements that generated the empirical correlation data that is used for the modeling of the convective heat transfer. A further source of discrepancy is the manufacturing tolerances, which lead to the deviation of the actual geometries from the assumed ones. Moreover, the epoxy casting process is found not to result in

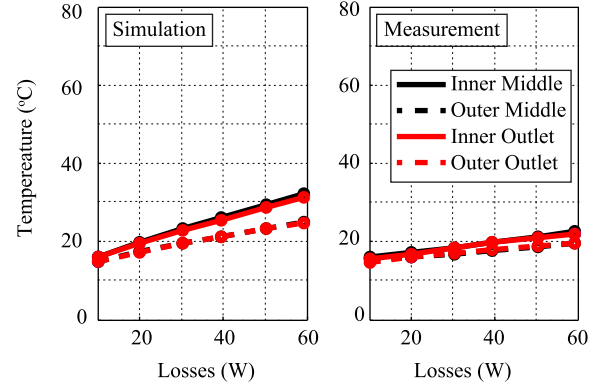


Fig. 11. Simulated and measured winding temperatures for axial duct cooling and 1 l/min water flow. Solid lines denote inner and dashed lines denote outer sensors (radial direction). Black denotes middle and red denotes outlet side (axial direction). The slopes of the measured lines are approximately 50% of the simulated lines, meaning that the models are over conservative for this particular case. The mismatch between the simulated and measured temperatures is 10 °C for the radially inner and 5 °C for radially outer sensor locations at 60 W.

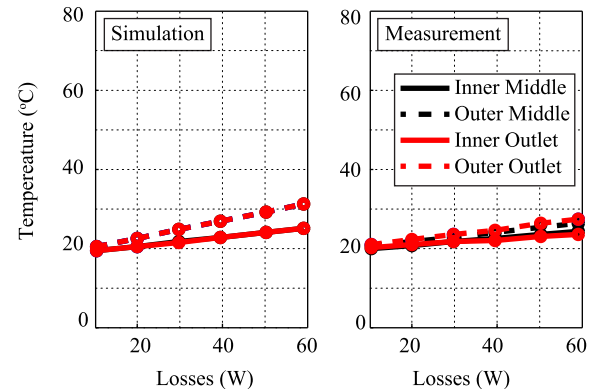


Fig. 12. Simulated and measured winding temperatures for annular gap cooling and 1 l/min water flow. Solid lines denote inner and dashed lines denote outer sensors (radial direction). Black denotes middle and red denotes outlet side (axial direction). The relative difference of the simulated and measured slopes is 25% for the radially outwards sensor locations. The difference between the measured and simulated hotspot temperatures is 4 °C at 60 W.

a homogeneously potted winding pack in some cases. This not only leads to a difference between the simulated and measured thermal paths, but also endangers the safe operation of the machine due to local hotspot risks, and therefore, the selection of the epoxy and the casting process shall be revisited within the course of future work. Nevertheless, both the models and the measurement results show a clear improvement of the cooling performance when axial ducts or an annular gap is used. Therefore, the design of an high-speed electrical machine with integrated cooling channels is discussed in the following section.

IV. FUNCTIONAL PROTOTYPE WITH INTEGRATED COOLING

A. Integrated Design Method

In the literature, several (semi-) analytical electromagnetic models have been proposed for slotless high-speed machines [32]–[34]. The computational effectiveness of the thermal modeling approach adopted in this work makes its coupling to such

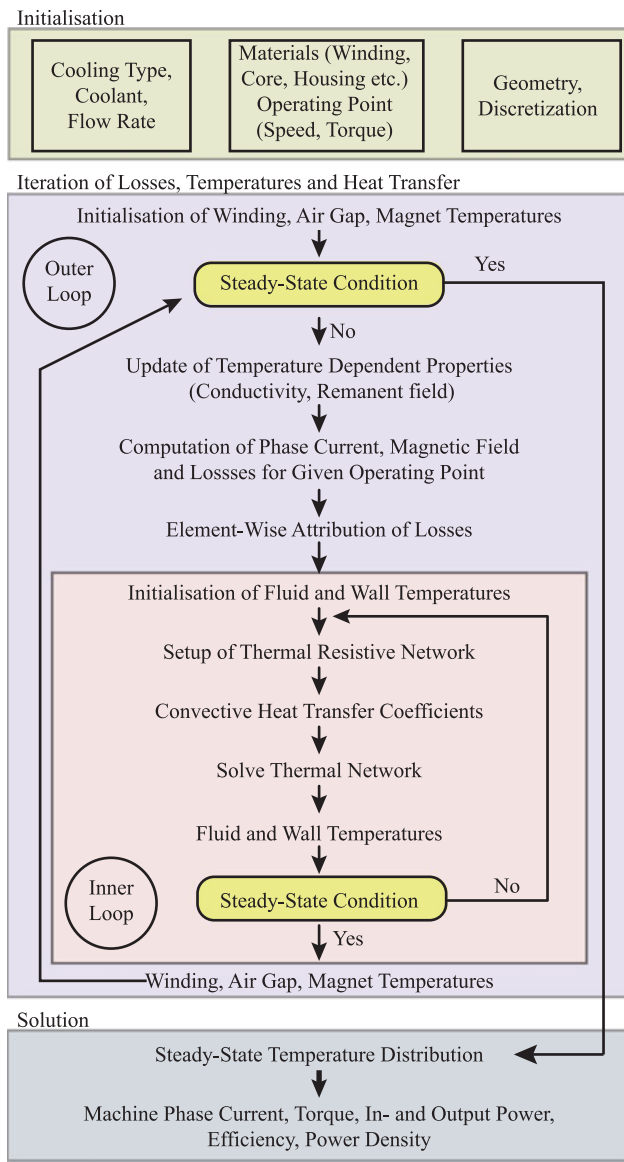


Fig. 13. Coupled thermal-electromagnetic design flow of a slotless, high-speed permanent magnet electrical machine. The computational efficiency of the model enables its use in a multiobjective optimization phase, where hundreds of iterations may be required.

models possible, which allows for a simultaneous optimization of the thermal and electromagnetic properties of the electrical machine. Especially in high-speed machines, mechanical models analyzing the mechanical stresses in the rotor and the rotor dynamics should also be integrated into the design procedure in order to avoid mechanical failure [35]. Nevertheless, since a new rotor design is not carried out in this work, mechanical modeling is not considered.

Fig. 13 shows the combined thermal-electromagnetic design work flow. Due to the bidirectional couplings between the thermal and electromagnetic domains, and between the temperature difference and the heat transfer coefficient at the solid–fluid interfaces, the model contains two cascaded iterative loops.

First, the machine to be analyzed is defined by defining its geometry and materials. After the operating point (speed and

torque) are set as model inputs, the cooling system is also defined at this stage by choosing the cooling type, the coolant, and its flow rate. The analysis starts by the initialization of the machine temperature, such that temperature-dependent electromagnetic parameters as the copper conductivity and PM remanent field can be defined. Based on those, the current for generating the desired torque, the resulting copper losses, as well as the core and windage losses are calculated according to [32]. In the next step, the losses are assigned to the relevant nodes in the thermal model, and the inner loop of iteration is executed by updating the thermal resistances that model the convective heat transfer, until they converge. This is fed back to the outer loop where the convergence of winding, air gap, and magnet temperatures is targeted. The resulting currents and efficiency are finally calculated based on the steady-state temperature distribution.

B. Improved Design and Hardware Construction

The two integrated cooling methods using axial ducts and annular gaps both lead to similar cooling performance. However, the annular gap requires smaller modifications in the winding production steps; hence, it is preferred due to the ease of manufacturing. A further advantage of the annular gap cooling is its ability to also cool the rotor better than the other methods, as the cooling channel is the closest to the air gap. This advantage becomes even more prominent when comparing to different cooling approaches not considered here, e.g., an axial housing flange thermally coupled to the end windings. For these reasons, the annular gap structure is chosen for further evaluation against the state-of-the-art jacket cooling in a functional machine prototype.

The mechanical design of the annular gap is adapted at this stage to improve its robustness. In the design described above, the cooling channel is formed between a plastic can that separates it from the air gap, and the winding pack comprising the conductors and epoxy. In other words, the coolant wets the winding pack directly. Even though this leads to a favorable cooling performance, the interaction of the coolant and the winding pack may endanger the safe operation of the machine, e.g., depending on the epoxy's chemical stability in the coolant. Therefore, an additional can with 0.6 mm wall thickness is introduced, such that the annular gap is formed between two plastic cans, one separating it from the air gap, the other from the winding pack. These cans are made of a thermoplastic, which features good dimensional stability in water and a thermal conductivity of 0.82 W/mK.

Fig. 14 compares the power-efficiency relationships of the jacket-cooled machine analyzed in this work and an annular-gap-cooled machine with the same rotor, the same stator core, and a 0.5 mm annular gap, as calculated by the model depicted in Fig. 13. When a constant copper fill factor of 0.3 is assumed, the introduction of an annular gap leads to a lower copper cross-sectional area, and consequently to a lower efficiency. On the other hand, a significantly higher amount of heat can be dissipated, leading to a power output increase of nearly 100% when the maximum winding temperature is limited to 80 °C (1000 W with jacket cooling versus 2000 W with annular gap), or in ex-

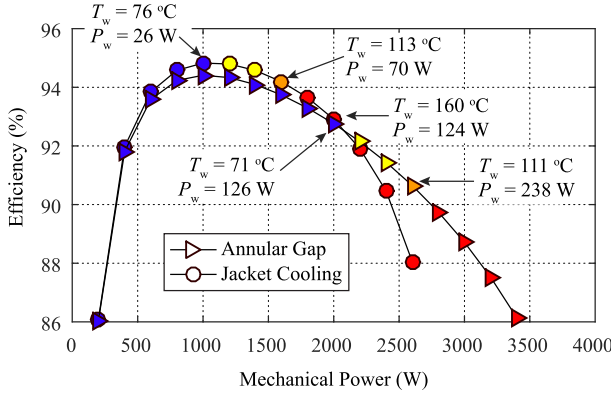


Fig. 14. Efficiency, power output, winding hotspot temperature (T_w), and copper losses (P_w) of machines featuring jacket cooling (circle) and 0.5 mm annular gap (triangle). The steeper decrease in efficiency in the case of jacket cooling is due to the higher winding and permanent-magnet temperatures of that machine compared to the machine featuring annular gap cooling. Blue color denotes $T_w < 80^\circ$, yellow $80^\circ < T_w < 100^\circ$, orange $100^\circ < T_w < 120^\circ$, and red $T_w > 120^\circ$.

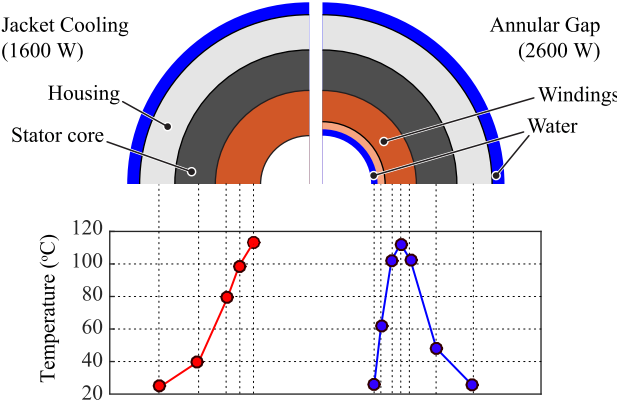


Fig. 15. Simulated temperature distribution at the axial middle of the machines with jacket and annular gap cooling, with output powers of 1600 and 2600 W, respectively.

cess of 60% when the maximum winding temperature is 120°C (1600 W with cooling jacket versus 2600 W with annular gap). The power requirement of the cooling system is not accounted for in this analysis.

Fig. 15 shows simulation results showing the calculated temperature distribution in the axial middle of both machines, for the operating points denoted with orange color in Fig. 14 (1600 W for the machine with jacket cooling and 2600 W for annular gap cooling). For the case of jacket cooling, the thermal resistivity of the winding pack plays an important role in determining the hotspot temperature; hence, investigating ways of increasing its thermal conductivity and having better thermal interfaces between different machine domains could potentially improve the thermal performance. For the annular gap cooling, the thermal resistance of the plastic can comes out as a significant parameter, hence a thinner can and/or a plastic can made of a material with higher thermal conductivity would lead to a better cooling performance.

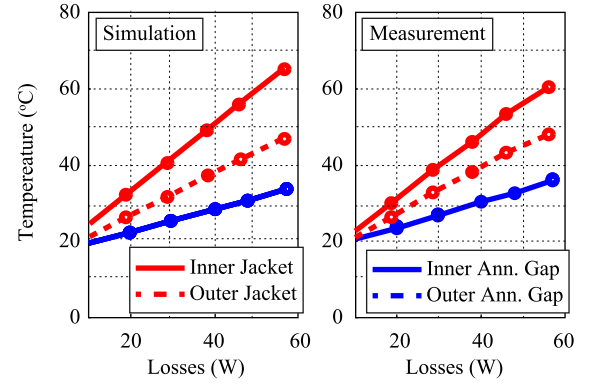


Fig. 16. Simulated and measured winding temperatures for jacket- and annular-gap-cooled machine prototypes, when they are heated with dc copper losses at standstill. Coolant is water with 1 l/min flow rate. Blue color denotes the machine with annular gap and red color denotes the machine with jacket cooling. Solid lines denote radially inside and dashed lines denote radially outside temperature sensor locations. For annular gap cooling, the radially in- and outside temperatures are at very similar values.

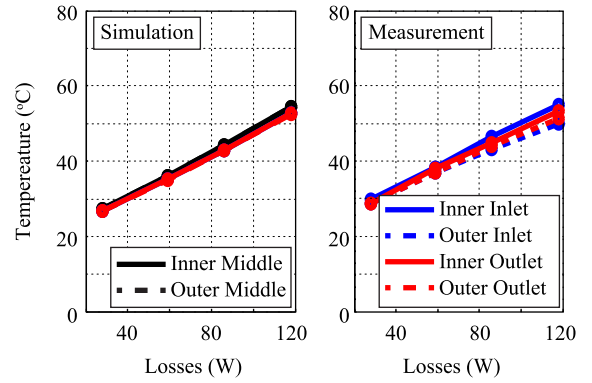


Fig. 17. Simulated and measured winding temperatures for the machine with annular gap cooling. The machine is heated with dc copper losses at standstill. Coolant is water with 1 l/min flow rate. Blue and red colors denote axial ends, and black color (only applicable to simulations) denotes the axial middle. Solid lines denote radially inside and dashed lines denote radially outside positions. The simulations predict a slope of $0.2854^\circ\text{C}/\text{W}$ whereas a maximum slope of $0.2793^\circ\text{C}/\text{W}$ and a minimum slope of $0.2333^\circ\text{C}/\text{W}$ are measured at the inner inlet and outer inlet sensor locations, resulting in relative errors of 2% and 18%, respectively.

C. Experimental Results

For a final verification of the models, two fully functional electrical machine prototypes are built according to Table I, one featuring jacket cooling and the other annular gap cooling. The outer housing dimensions as well as the coolant inlet and outlet connectors are kept the same in both machines. Both are again equipped with the temperature sensors previously described.

Fig. 16 shows simulated and measured winding temperatures for jacket- and annular-gap-cooled machine prototypes, when they are heated with up to 60 W dc copper losses at standstill. For this test, the rotor is not mounted, and the heat transfer through air gap is not modeled in the corresponding simulation. More than 20°C winding hotspot temperature reduction is seen with the annular gap cooling. The same test is repeated in Fig. 17 up to 120 W of losses for the machine with annular gap cooling, where the recorded maximum winding temperature is below

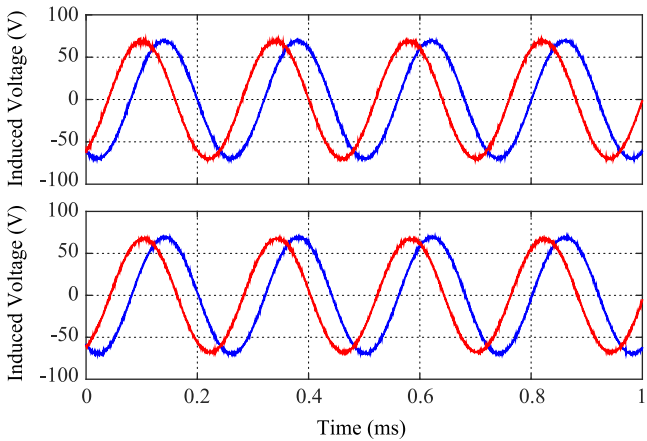


Fig. 18. Back-EMF of the machines with jacket cooling (top) and annular gap cooling (bottom) at 250 000 r/min. Voltages are measured line-to-line on two machine terminals with respect to the third terminal.

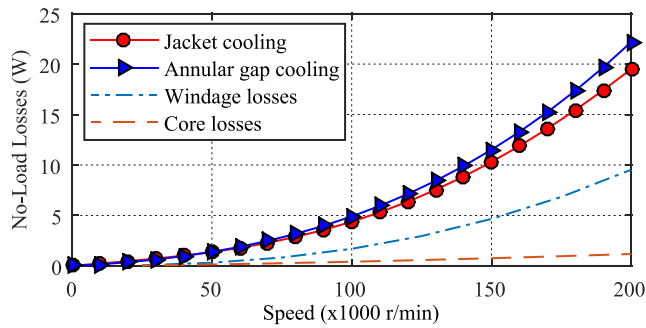


Fig. 19. The measured no-load losses for the machines with jacket cooling and annular gap cooling, as well as the calculated windage and stator core losses. The difference between the measured losses and the sum of windage and stator core losses is attributed to the bearing losses.

what has been recorded with the jacket-cooled machine at only 60 W.

Fig. 18 shows the measured induced voltage [(back-electromotive force (EMF)] for both machines under no load at 250 000 r/min. Finally, the no-load losses, which are measured with deceleration tests [36], are shown in Fig. 19. Featuring the same rotor and stator core, and mechanical air gap geometries, the two machine prototypes are expected to have the same no-load losses. Therefore, the difference in the measured losses is attributed to the manufacturing tolerances, e.g., of the bearing housings.

V. CONCLUSION

Slotless PM electrical machines have been the machine of choice for high-speed drives above 200 000 r/min, due to their lower rotor losses. The latter also means magnetic limits such as PM demagnetization or stator core saturation are hard to reach in practical machine designs. Hence, the maximum power output of the machine is generally set by thermal limits. In certain applications, the power density of the electrical machine plays a very important role, and a lower machine efficiency may be tolerated in order to have a higher power output from

a machine with a given volume. Therefore, different forced cooling methods are discussed in this work with the goal of increasing the power output of the electrical machine.

A lumped-parameter-based modeling approach is adopted to study the thermal behavior of the machines with different forced cooling methods. The presented models are flexible, sufficiently accurate, and at the same time computationally very efficient. This enables their coupling with electromagnetic models and incorporation into the machine optimization procedure.

In order to verify the discussed cooling concepts in hardware, different stators featuring different cooling concepts are manufactured. Based on initial measurements on these stators, the thermal models are verified, and an annular cooling gap on the inner surface of the winding pack is identified as the most promising integrated forced cooling method.

A coupled thermal-electromagnetic model is developed, and is used to predict the power versus efficiency relationship of machines employing jacket and annular gap cooling. For the analyzed machine, a power density increase of nearly 100% is possible simply by the integration of the cooling channel into the machine instead of using a standard cooling jacket, when the same stator core and the same rotor is used and the maximum winding temperature is kept below 80 °C. Two fully functional electrical machines are manufactured featuring jacket and annular gap cooling, and used to verify the electromagnetic and (once more) the thermal models.

It is also worth noting that even if the power density increase is not a major concern, an integrated cooling method may be employed to decrease the winding hotspot temperature, and alleviate the negative effects of thermal cycling. To that end, the future work shall focus on extending the models to study also the transient thermal behavior of such machines, in order to assess their intermittent overloading capacities. The power requirement of different cooling systems shall also be studied.

REFERENCES

- [1] D. Gerada, A. Mebarki, N. L. Brown, C. Gerada, A. Cavagnino, and A. Boglietti, "High-speed electrical machines: Technologies, trends, and developments," *IEEE Trans. Ind. Electron.*, vol. 61, no. 6, pp. 2946–2959, Jun. 2014.
- [2] T. Baumgartner and J. W. Kolar, "Multivariable state feedback control of a 500 000-r/min self-bearing permanent-magnet motor," *IEEE/ASME Trans. Mechatronics*, vol. 20, no. 3, pp. 1149–1159, Jun. 2015.
- [3] A. Looser and J. W. Kolar, "An active magnetic damper concept for stabilization of gas bearings in high-speed permanent-magnet machines," *IEEE Trans. Ind. Electron.*, vol. 61, no. 6, pp. 3089–3098, Jun. 2014.
- [4] A. S. de Lacerda Costa, R. R. Bastos, S. da Costa Paolinelli, S. L. Nau, R. M. Valle, and B. de Jesus Cardoso Filho, "Characterization of electrical steels for high-speed induction motors applications: Going beyond the common practices," *IEEE Trans. Ind. Appl.*, vol. 52, no. 2, pp. 1350–1358, Mar. 2016.
- [5] A. Tüysüz, M. Schöni, and J. W. Kolar, "Novel signal injection methods for high speed self-sensing electrical drives," in *Proc. IEEE Energy Convers. Congr. Expo.*, Sep. 2012, pp. 4663–4670.
- [6] C. Zwyssig, S. D. Round, and J. W. Kolar, "An ultrahigh-speed, low power electrical drive system," *IEEE Trans. Ind. Electron.*, vol. 55, no. 2, pp. 577–585, Feb. 2008.
- [7] A. Borisavljevic *et al.*, "Motor drive for a novel high-speed micro-milling spindle," in *Proc. IEEE/ASME Int. Conf. Adv. Intell. Mechatronics*, Jul. 2009, pp. 1492–1497.
- [8] D. Krähenbühl, C. Zwyssig, H. Weser, and J. W. Kolar, "A miniature 500 000-r/min electrically driven turbocompressor," *IEEE Trans. Ind. Appl.*, vol. 46, no. 6, pp. 2459–2466, Nov. 2010.

- [9] C. Zwyssig, T. Baumgartner, and J. W. Kolar, "High-speed magnetically levitated reaction wheel demonstrator," in *Proc. Int. Power Electron. Conf.*, May 2014, pp. 1707–1714.
- [10] A. Boglietti, A. Cavagnino, and D. Staton, "Determination of critical parameters in electrical machine thermal models," *IEEE Trans. Ind. Appl.*, vol. 44, no. 4, pp. 1150–1159, Jul. 2008.
- [11] D. G. Dorrell, "Combined thermal and electromagnetic analysis of permanent-magnet and induction machines to aid calculation," *IEEE Trans. Ind. Electron.*, vol. 55, no. 10, pp. 3566–3574, Oct. 2008.
- [12] S. A. Semidey, Y. Duan, J. R. Mayor, R. G. Harley, and T. G. Habetler, "Optimal electromagnetic-thermo-mechanical integrated design candidate search and selection for surface-mount permanent-magnet machines considering load profiles," *IEEE Trans. Ind. Appl.*, vol. 47, no. 6, pp. 2460–2468, Nov. 2011.
- [13] W. Jiang and T. M. Jahns, "Coupled electromagnetic-thermal analysis of electric machines including transient operation based on finite-element techniques," *IEEE Trans. Ind. Appl.*, vol. 51, no. 2, pp. 1880–1889, Mar. 2015.
- [14] M. Popescu, D. A. Staton, A. Boglietti, A. Cavagnino, D. Hawkins, and J. Goss, "Modern heat extraction systems for power traction machines—A review," *IEEE Trans. Ind. Appl.*, vol. 52, no. 3, pp. 2167–2175, May 2016.
- [15] A. Tüysüz, M. Steichen, C. Zwyssig, and J. W. Kolar, "Advanced cooling concepts for ultra-high-speed machines," in *Proc. Int. Conf. Power Electron.*, Jun. 2015, pp. 2194–2202.
- [16] A. Boglietti, A. Cavagnino, D. Staton, M. Shanel, M. Mueller, and C. Mejuto, "Evolution and modern approaches for thermal analysis of electrical machines," *IEEE Trans. Ind. Electron.*, vol. 56, no. 3, pp. 871–882, Mar. 2009.
- [17] B. Zhang, R. Qu, J. Wang, W. Xu, X. Fan, and Y. Chen, "Thermal model of totally enclosed water-cooled permanent-magnet synchronous machines for electric vehicle application," *IEEE Trans. Ind. Appl.*, vol. 51, no. 4, pp. 3020–3029, Jul. 2015.
- [18] R. Wrobel and P. H. Mellor, "A general cuboidal element for three-dimensional thermal modelling," *IEEE Trans. Magn.*, vol. 46, no. 8, pp. 3197–3200, Aug. 2010.
- [19] N. Simpson, R. Wrobel, and P. H. Mellor, "A general arc-segment element for three-dimensional thermal modeling," *IEEE Trans. Magn.*, vol. 50, no. 2, pp. 265–268, Feb. 2014.
- [20] A. Looser, T. Baumgartner, J. W. Kolar, and C. Zwyssig, "Analysis and measurement of three-dimensional torque and forces for slotless permanent-magnet motors," *IEEE Trans. Ind. Appl.*, vol. 48, no. 4, pp. 1258–1266, Jul. 2012.
- [21] Celeroton AG, Volketswil, Switzerland, Permanent-magnet motor CM-25-280 (Datasheet). 2016. [Online]. Available: www.celeroton.com
- [22] R. M. Burkart, H. Uemura, and J. W. Kolar, "Optimal inductor design for 3-phase voltage-source PWM converters considering different magnetic materials and a wide switching frequency range," in *Proc. Int. Power Electron. Conf.*, May 2014, pp. 891–898.
- [23] Matweb database of material properties. Overview of materials for aluminum alloy (Data chart). 2016. [Online]. Available: www.matweb.com
- [24] 3M, Maplewood, MI, USA, Thermally conductive epoxy adhesives (Datasheet). 2016. [Online]. Available: solutions.3m.com
- [25] A. Materials, Lake City, FL, USA, Titanium alloy properties (material data chart). 2016. [Online]. Available: www.azom.com
- [26] Bomatec AG, Hori, Switzerland, SmCo 2:17 sintered permanent magnets (Datasheet). 2016. [Online]. Available: www.bomatec.ch
- [27] M. Schrittwieser, A. Marn E. Farnleitner, and G. Kastner, "Numerical analysis of heat transfer and flow of stator duct models," *IEEE Trans. Ind. Appl.*, vol. 50, no. 1, pp. 226–233, Jan. 2014.
- [28] Verein Deutsche Ingenieure (VDI), *Wärmeatlas*, (in German). Berlin, Germany: Springer-Verlag, 2009.
- [29] P. R. N. Childs and C. A. Long, "A review of forced convective heat transfer in stationary and rotating annuli," *J. Mech. Eng. Sci.*, vol. 210, no. 2, pp. 123–134, Mar. 1996.
- [30] J. Nerg, M. Rilla, and J. Pyrhonen, "Thermal analysis of radial-flux electrical machines with a high power density," *IEEE Trans. Ind. Electron.*, vol. 55, no. 10, pp. 3543–3554, Oct. 2008.
- [31] M. Schiefer and M. Doppelbauer, "Indirect slot cooling for high-power-density machines with concentrated winding," in *Proc. IEEE Int. Elect. Mach. Drives Conf.*, May 2015, pp. 1820–1825.
- [32] J. Luomi, C. Zwyssig, A. Looser, and J. W. Kolar, "Efficiency optimization of a 100-W 500 000-r/min permanent-magnet machine including air-friction losses," *IEEE Trans. Ind. Appl.*, vol. 45, no. 4, pp. 1368–1377, Jul. 2009.
- [33] P. D. Pfister and Y. Perriard, "Slotless permanent-magnet machines: General analytical magnetic field calculation," *IEEE Trans. Magn.*, vol. 47, no. 6, pp. 1739–1752, Jun. 2011.
- [34] S. Jumayev, K. O. Boynov, J. J. H. Paulides, E. A. Lomonova, and J. Pyrhonen, "Slotless PM machines with skewed winding shapes: 3D electromagnetic modeling," *IEEE Trans. Magn.*, vol. 52, no. 11, Nov. 2016, Art. no. 8108212.
- [35] A. Borisavljevic, H. Polinder, and J. A. Ferreira, "On the speed limits of permanent-magnet machines," *IEEE Trans. Ind. Electron.*, vol. 57, no. 1, pp. 220–227, Jan. 2010.
- [36] A. Tüysüz, C. Zwyssig, and J. W. Kolar, "A novel motor topology for high-speed micro-machining applications," *IEEE Trans. Ind. Electron.*, vol. 61, no. 6, pp. 2960–2968, Jun. 2014.



Arda Tüysüz (S'10–M'13) received the B.Sc. degree in electrical engineering from Istanbul Technical University, Istanbul, Turkey, in 2006; the M.Sc. degree in electrical power engineering from RWTH Aachen University, Aachen, Germany, in 2009; and the Ph.D. degree in electrical drives from the Swiss Federal Institute of Technology (ETH) Zurich, Zurich, Switzerland, in 2015.

He is currently a Postdoctoral Researcher with the Power Electronic Systems Laboratory, ETH Zurich. His research interests include novel electrical machine topologies, self-sensing control of high-speed electrical machines, and wide-bandgap power devices for very efficient and compact electrical drive systems.



Francesca Meyer received the B.Sc. degree in mechanical engineering, and the M.Sc. degree in energy science and technology from the Swiss Federal Institute of Technology (ETH) Zurich, Zurich, Switzerland, in 2014 and 2016, respectively. She is currently with ABB Switzerland, Baden, Switzerland.



Mathis Steichen received the M.Sc. degree in electrical engineering and information technology from the Swiss Federal Institute of Technology (ETH) Zurich, Zurich, Switzerland, in 2014. He is currently working toward the Ph.D. degree at the Interdisciplinary Center for Security, Reliability, and Trust (SnT), University of Luxembourg, Luxembourg.



Christof Zwysig (M'10) received the M.Sc. and Ph.D. degrees in electrical engineering from the Swiss Federal Institute of Technology (ETH) Zurich, Zurich, Switzerland, in 2004 and 2008, respectively.

He was at the Chalmers University of Technology, Gothenburg, Sweden, where he was involved in the field of wind turbines. Since 2009, he has been with Celeroton AG, Zurich, a spin-off company in the area of high-speed electrical drive systems, of which he is a Co-founder.



Johann W. Kolar (F'10) received the M.Sc. and Ph.D. degrees (summa cum laude/promotio sub auspiciis praesidentis rei publicae) from the University of Technology Vienna, Vienna, Austria, in 1997 and 1999, respectively.

Since 1984, he has been working as an Independent Researcher and International Consultant in close collaboration with the University of Technology Vienna in the fields of power electronics, industrial electronics, and high-performance drives. He initiated and/or is the Founder of four ETH Spin-off companies. He has proposed numerous novel pulse-width modulation converter topologies and modulation and control concepts, and has supervised over 60 Ph.D. students. He has published more than 650 scientific papers in international journals and conference proceedings, 3 book chapters, and has filed more than 120 patents. The focus of his current research is on ultracompact and ultraefficient SiC and GaN converter systems, wireless power transfer, solid-state transformers, power supplies on chip, and ultra-high speed and bearingless motors.

Dr. Kolar has received 23 IEEE Transactions and Conference Prize Paper Awards, the 2014 IEEE Middlebrook Award, and the ETH Zurich Golden Owl Award for excellence in teaching. He is a member of the steering committees of several leading international conferences in the field and has served from 2001 through 2013 as an Associate Editor of the IEEE TRANSACTIONS ON POWER ELECTRONICS. Since 2002, he has been an Associate Editor of the *Journal of Power Electronics of the Korean Institute of Power Electronics* and is a Member of the Editorial Advisory Board of the *IEEJ Transactions on Electrical and Electronic Engineering*.